The Japan Society of Mechanical Engineers



# Molecular Dynamics Simulations of Shape-Memory Behavior Based on Martensite Transformation and Shear Deformation*

Takuya UEHARA**, Takato TAMAI*** and Nobutada OHNO****

Molecular dynamics simulations of the shape-memory effect are carried out to investigate the atomistic behavior during deformation and shape-recovery processes. The embedded-atom-method potential function and parameters for Ni-Al alloy are applied. The initial configurations of atoms are set on the lattice points of the martensite structure, in which the distribution of the variant orientation is limited to the two-dimensional direction for simplicity. When the shear load is imposed toward the $x$ direction, parallel to the variant interface, the deformation of the variants occurs, and finally, all variants settle into the uniform orientation. The deformed state is maintained after the load is released, and the original shape is recovered through heating and cooling processes because of phase transformation to bcc and martensite. In the loading process, the stress-strain curve exhibits a zigzag shape consisting of repeated stress increase and abrupt release. The interval of the stress peaks is revealed to be smaller as the model size becomes larger. Deformation observed in variant layers seems to occur at the same time at every points in the layer for a small model. However, the simulation with a large model indicates a nucleation and propagation behavior in each layer.

***Key Words:*** Molecular Dynamics, Shape-Memory Alloy, Phase Transformation, Martensite, Computer Simulation

## 1. Introduction

The shape-memory effect is one of the most typical phenomena in which the microscopic structure of the material influences the macroscopic behavior. The simulation model for the shape-memory effect has been developed by Tanaka and Nagaki[1] based on the constitutive equations of the continuum mechanical framework, and the numerical analyses by the finite element method have successfully demonstrated the deformation of shape-memory materials. Such volumetrically averaged properties, however, miss the microstructure-based phenomena. Therefore, a model that directly considers the microstructure in the material is required.

At the atomistic level, the shape memory behavior is related to the phase transformation and deformation of martensite variants. The schematic illustration is shown in Fig. 1. In this typical mechanism of shape-memory alloy (SMA), the bcc structure is stable at high temperature. When it is cooled to a low temperature, phase transformation to martensite, which consists of randomly orientated variants, occurs. When external force is imposed on the model, macroscopic deformation is induced by the change in direction of the variants. This process is irreversible, except for elastic recovery, and a permanent deformation is generated. The original shape with randomly orientated martensite variants is recovered through heating and cooling processes. Once the phase transformation to bcc occurs upon heating, the direction of all variants is reset, which are again oriented randomly during martensite transformation upon cooling.

While the aforementioned mechanism is well known, the direct in-situ observation of the atomistic process has not been demonstrated yet due to the difficulty of ex-

* Received 29th November, 2005 (No. 05-4263)

** Department of Computational Science and Engineering, Nagoya University, Furo-cho, Chikusa-ku, Nagoya 464–8603, Japan. E-mail: uehara@mech.nagoya-u.ac.jp

*** Department of Energy Conversion Science, Kyoto University, Yoshida Hon-machi, Sakyo-ku, Kyoto 606–8501, Japan

**** Department of Computational Science and Engineering, Nagoya University, Furo-cho, Chikusa-ku, Nagoya 464–8603, Japan



NII-Electronic Library Service

The Japan Society of Mechanical Engineers



Table 1 EAM parameters for Ni and Al in units of eV for energy and Å for length (I)

| | $Z_0$ | $\alpha$ | $\beta$ | $\nu$ | $N^s$ | $N^d$ | $k_1$ | $k_2$ | $k_3$ |
|---|---|---|---|---|---|---|---|---|---|
| Ni | 10 | 1.554 | 0.352 | 0.5 | 1.7 | 8.3 | -26.883 | -34.040 | -75.016 |
| Al | 3 | 1.3 | 1.5 | 0.5 | 0.76 | 2.24 | -33.372 | 43.995 | -186.75 |

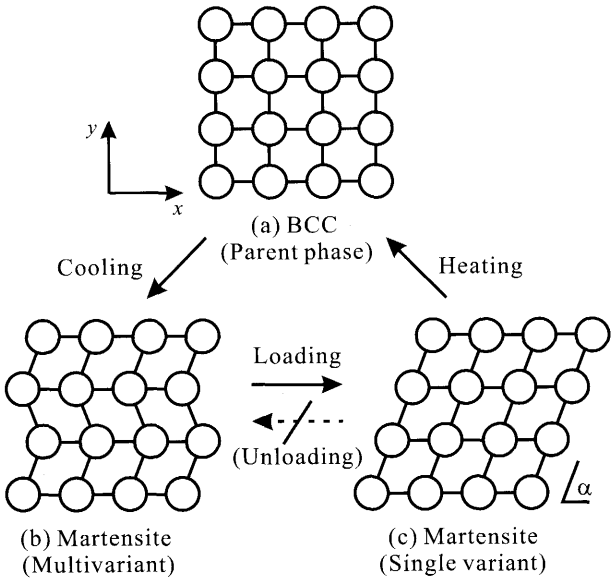


Fig. 1 Illustration of the shape-memory effect related with martensitic transformation

tremely small length and time scales. Therefore, computer simulations are expected for clarifying the mechanism, and the molecular dynamics (MD) method is considered to be suitable for this purpose. As an example of SMA, we focus on Ni-Al alloy, since several researchers have reported MD simulations of martensite structures. For example, Foiles and Daw[2], and Chen et al.[3] have demonstrated the stable structure of $Ni_3Al$ by using the embedded-atom-method (EAM) potential function with suitable parameters[4),(5)]. Rubini and Ballone[6] and Farkas et al.[7] have also reported that the bcc and martensite structures are reproduced using the EAM potential. Hence the authors have performed molecular dynamics simulations of the shape memory effect using the EAM potential, by applying a series of loading, unloading, heating and cooling to a simple model[8)-(10)]. However, only a small model was used in previous studies, and the influence of the model size was not clarified. In this study, therefore, we extend the simulation by using models of different sizes, and discuss the size dependence of the stress-strain curves. The local deformation process in the martensite variants is also demonstrated.

## 2. Molecular Dynamics Method

In the classical molecular dynamics method, the following Newton's equation of motion for every atom in the system considered is numerically solved.

Table 2 EAM parameters (II)

| Ni | | | | Al | | | |
|---|---|---|---|---|---|---|---|
| $I$ | $n_I$ | $\zeta_I$ | $C_I$ | $I$ | $n_I$ | $\zeta_I$ | $C_I$ |
| s 1 | 1 | 54.88885 | -0.00389 | s 1 | 1 | 26.89394 | -0.00452 |
| 2 | 1 | 38.48431 | -0.02991 | 2 | 1 | 20.27618 | 0.08395 |
| 3 | 2 | 27.42703 | -0.03189 | 3 | 2 | 9.45860 | -0.11622 |
| 4 | 2 | 20.88204 | 0.15289 | 4 | 2 | 6.86435 | -0.18811 |
| 5 | 3 | 10.95707 | -0.20048 | 5 | 3 | 3.35342 | 0.54265 |
| 6 | 3 | 7.31958 | -0.05423 | 6 | 3 | 2.09388 | 0.55020 |
| 7 | 4 | 3.9265 | 0.49292 | p 1 | 2 | 13.62535 | -0.04475 |
| 8 | 4 | 2.15289 | 0.61875 | 2 | 2 | 6.90762 | -0.14977 |
| d 1 | 3 | 12.67582 | 0.4212 | 3 | 3 | 3.18100 | 0.26788 |
| 2 | 3 | 5.43253 | 0.70658 | 4 | 3 | 1.72743 | 0.80384 |

$$m_i\ddot{\boldsymbol{r}}_i = \boldsymbol{f}_i = -\frac{\partial \Phi}{\partial \boldsymbol{r}_i} \tag{1}$$

Here, $\boldsymbol{f}_i$ is the force acting on the $i$-th atom, $\Phi$ is the potential energy of the system, and $m_i$ and $\boldsymbol{r}_i$ are the mass and position vector of the $i$-th atom, respectively. Using the embedded atom method, the potential energy $\Phi$ is expressed as follows:

$$\Phi = \sum_i F(\rho_i) + \frac{1}{2}\sum_i \sum_{j\neq i} \phi_{ij}(r_{ij}). \tag{2}$$

Here, the first term is the many-body term with the embedding function $F$ as a function of the local electron density $\rho_i$ around the $i$-th atom, which is assumed to be expressed by

$$\rho_i = \sum_{j\neq i} \tilde{\rho}(r_{ij}) = \sum_{j\neq i} \{N^s \tilde{\rho}^s(r_{ij}) + N^d \tilde{\rho}^d(r_{ij})\}, \tag{3}$$

$$\tilde{\rho}^s(r_{ij}) = \tilde{\rho}^d(r_{ij}) = |\sum C_I R_I|^2 / 4\pi, \tag{4}$$

$$R_I = \frac{(2\zeta_I)^{n_I+1/2}}{[(2\zeta_I)]^{1/2}} r_{ij}^{n_I-1} \exp(-\zeta_I r_{ij}). \tag{5}$$

Here, $N^s$, $N^d$, $C_I$, $\zeta_I$ and $n_I$ are the parameters depending on the species of the atom; those for several metals have been listed by Clementi and Roetti[11]. We take the parameters for Ni and Al from their list, as shown in Tables 1 and 2, in which the values are given in units of eV and Å.

In order to determine the embedding function $F$, the universal function proposed by Rose et al.[12] is applied, and the following function is derived:

$$F(\rho) = k_1\rho^{1/2} + k_2\rho + k_3\rho^2, \tag{6}$$

where $k_1$, $k_2$, and $k_3$ are the parameters for Ni or Al, as listed in Table 1.

The second term of Eq. (2) is a two-body term as a function of the distance between two atoms $r_{ij}$, which is represented by

$$\phi_{ij}(r_{ij}) = Z_i(r_{ij})Z_j(r_{ij})/r_{ij}\,, \tag{7}$$

$$Z(r_{ij}) = Z_0(1+\beta r_{ij}^{\nu})\exp(-\alpha r_{ij}). \tag{8}$$

Here, $Z_0$, $\beta$, $\nu$ and $\alpha$ are the parameters for Ni and Al,



NII-Electronic Library Service

The Japan Society of Mechanical Engineers



which are also listed in Table 1.

## 3. Simulation Model and Conditions

### 3.1 Preliminary simulations

The set parameters in the previous section have been revealed to represent both the bcc and martensite phases between the Ni contents of 60% to 70%[9],[10]. Figure 2 (a) and (b) illustrates the configuration of atoms in the stable structure at low temperatures for Ni contents of 60% and 68%, respectively. The crystal structure for 60% Ni is body-centered cubic, and that for 68% Ni is a slightly inclined structure, which we call "martensite" in this study. The unit cell of each structure is illustrated in Fig. 3. The base square of the unit cell in the $x$–$y$ plane is identical for both structures, while the atoms in the middle layer are slid to the left along the $x$ axis, forming inclined layers, which we call "variant" in this study. This inclined direction is random, and the configuration in Fig. 2 (b) exhibits randomly accumulated variant layers, while the direction is consistent within each layer.

In our preliminary simulations[10], the dependence of the structure on temperature was also investigated. The martensite structure was, consequently, revealed to be stable at low temperatures, while the bcc structure is stable at high temperatures. This feature is most marked at around 68% Ni. This results are qualitatively consistent with those of experiments, and, therefore, we use the 68% Ni model in the shape-memory simulations.

### 3.2 Model and conditions

Figure 4 shows the profile of the simulation conditions. A series of simulations, consisting of 40 000 time steps, is divided into 4 stages: I. loading, II. unloading, III. heating and IV. cooling. In the loading stage I, shear deformation of the simulation model is forcibly imposed

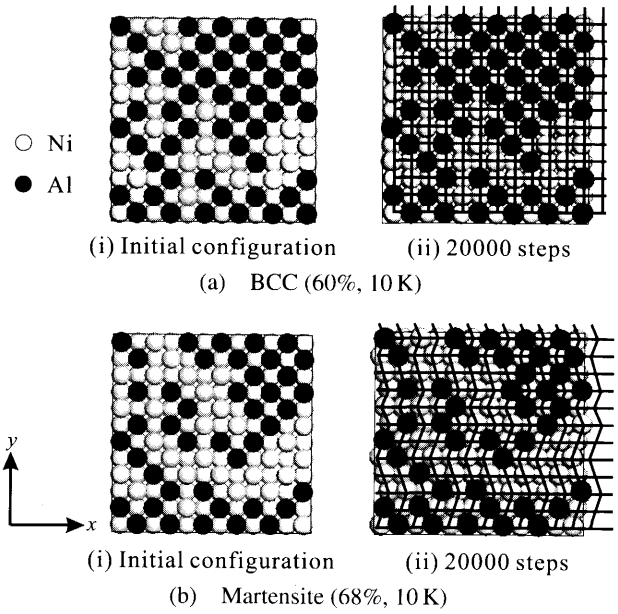


Fig. 2 Illustration of the bcc and martensite structures, which are obtained for 60% Ni and 68% Ni models, respectively

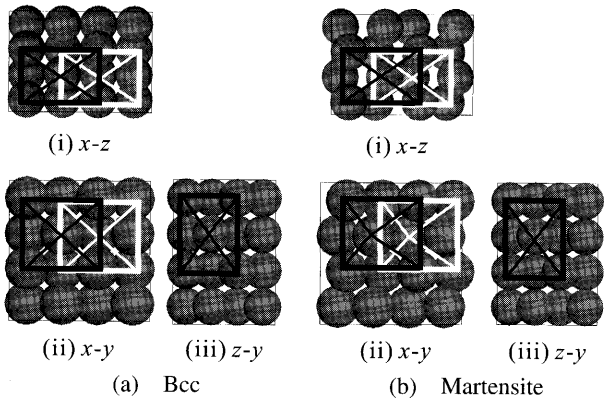


Fig. 3 Unit cells of bcc and martensite structures

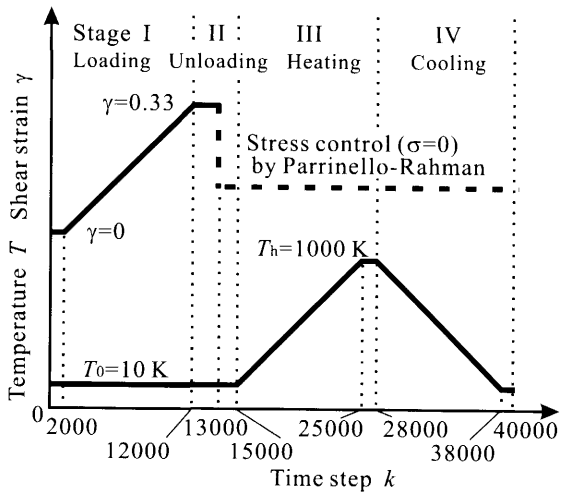


Fig. 4 Profile of the applied simulation conditions

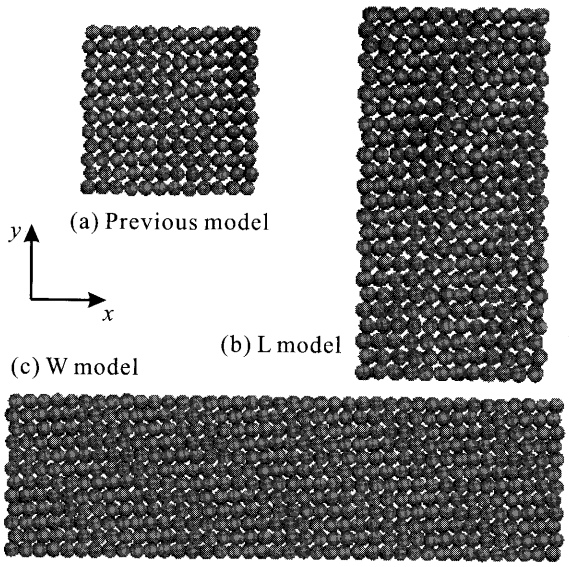


Fig. 5 Initial configurations of atoms for L model, W model and previously applied model



NII-Electronic Library Service

The Japan Society of Mechanical Engineers



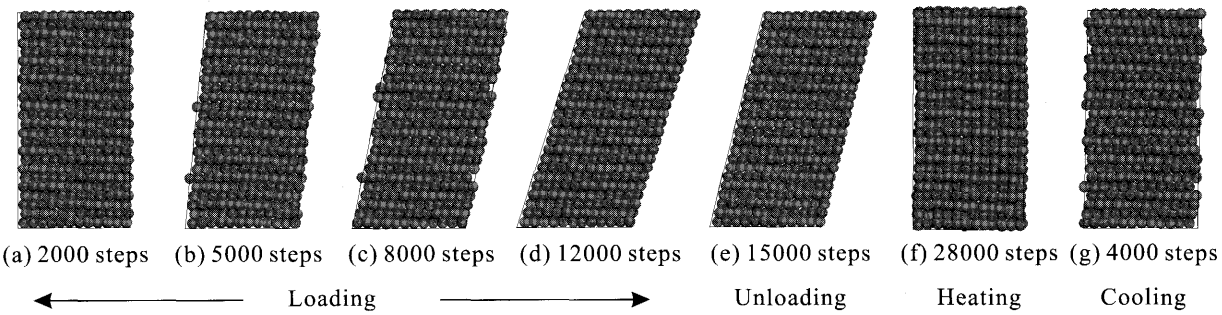


Fig. 6 Variation of the configuration of atoms in deformation and shape-recovery processes for L model

by tilting the $y$ axis of the model toward the $x$ direction until the shear strain $\gamma_{xy}$ reaches 0.33. The length of the edges along all directions are adjusted so that the axial stress component is kept at zero. The temperature of the system is controlled to be constant at $T = 10$ K by the velocity-scaling method. In the unloading stage II, the stress is released using the Parrinello-Rahman (PR) algorithm[13),(14)] at constant temperature. The model is allowed to change its shape such that all stress components including shear are zero. During the heating process, stage III, the temperature is raised continuously to $T = 1\,000$ K by the velocity-scaling method. The peak temperature, $T_h = 1\,000$ K, which should be sufficiently above the transformation temperature from martensite to bcc, is chosen on the basis of the results of the preliminary simulations. Finally, the model is cooled to the initial temperature of $T = 10$ K in stage IV. The stress is controlled to be zero by the PR method during heating and cooling processes.

Since we assumed the process corresponding to the illustration in Fig. 1, a simple model was applied in our previous simulations[9),(10)], where the size of the model was $6 \times 6 \times 6$ unit cells. In this study, we apply larger models, one of which is twice longer in the $y$ direction (L model), and another which is three-times wider in the $x$ direction (W model), as shown in Fig. 5. The atoms are placed on the lattice points of the martensite structure. Periodic boundary conditions for all directions are applied, and the time increment is chosen to be 1.5 fs.

## 4. Results and Discussion

### 4.1 Shear loading and unloading processes

Figure 6 represents the configuration of atoms through a simulation from stages I to IV with the L model, and Fig. 7 shows the stress-strain (S-S) curve for the corresponding processes.

When the shear strain is imposed on the model from the 2 000th time step, shear stress arises, as shown in Fig. 7, because of the elastic deformation. When the stress reaches about 2.5 GPa, it is abruptly released. As the strain is continuously imposed, the stress again starts increasing, and drastic release occurs again while the stress level is lower than that at the first drop. Similar behavior of the S-S curve, gradual increase and abrupt release, is observed repeatedly. The interval is almost constant, and the peaks of the stress rise as total strain becomes greater.

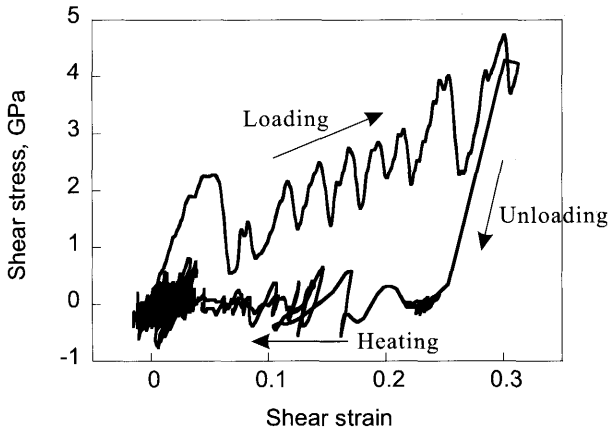


Fig. 7 Stress-strain curves in loading, unloading, heating and cooling processes, which indicate the shape-memory effect

This stress release is related to the deformation of the variant layers. At the initial configuration in Fig. 6 (a), the same number of variant layers are orientated to the right and left directions, and in the early stage, only elastic deformation is observed. However, in Fig. 6 (b), after the stress release, several layers exhibit the opposite direction from the original state, while the angle of the incline remains constant. The number of deformed layers increases as strain becomes greater, and finally, a single-variant martensite structure with a large deformation is obtained, as shown in Fig. 6 (d).

In the unloading process, the stress-control method is changed to the Parrinello-Rahman method. Then, the strain recovers slightly with an almost linear response of the stress, as shown in Fig. 7. This behavior clearly corresponds to elastic recovery, and a permanent strain remains.

From the results for stages I and II, this model is concluded to be in good agreement with the overall deformation process illustrated in Fig. 1, while atomistically specific behavior is observed.

### 4.2 Heating and cooling processes

When the temperature of the model is raised to



NII-Electronic Library Service

The Japan Society of Mechanical Engineers



$T$ = 1 000 K, the martensite structure transforms to the bcc structure. Since the bcc structure is homogeneous isotropic cubic, the shape is independent of the direction of the variant layers before the transformation. Therefore, the model is restored to the original undeformed state. The S-S curve shows the shift from $\gamma = 0.25$ to 0 with the stress kept at zero, except for fluctuation due to thermal vibrations.

In the cooling stage, martensite transformation occurs with random generation of variant orientation. Therefore, total deformation does not occur. This corresponds to the shape recovery upon heat treatment depicted in Fig. 1.

### 4.3 Size dependence of S-S curve

In order to show the size dependence of the results, the stress-strain curves are shown in Fig. 8, in which the solid line is the result for the previously used small model (model (a) in Fig. 5), and the dashed line is for the L model in this study. The gradients of the curves in the early stage are identical to each other, which indicates that the elastic modulus is independent of the model size. The initial stress peak is slightly higher for the larger model, while the outlines of the S-S curves show similar tendencies with repeated gradual stress increase and abrupt release. However, the interval of stress release and the step height in the S-S curve are smaller for the larger model. This tendency indicates that the zigzag S-S curve on the atomistic scale approaches a continuous one on the macroscale as the model size becomes larger.

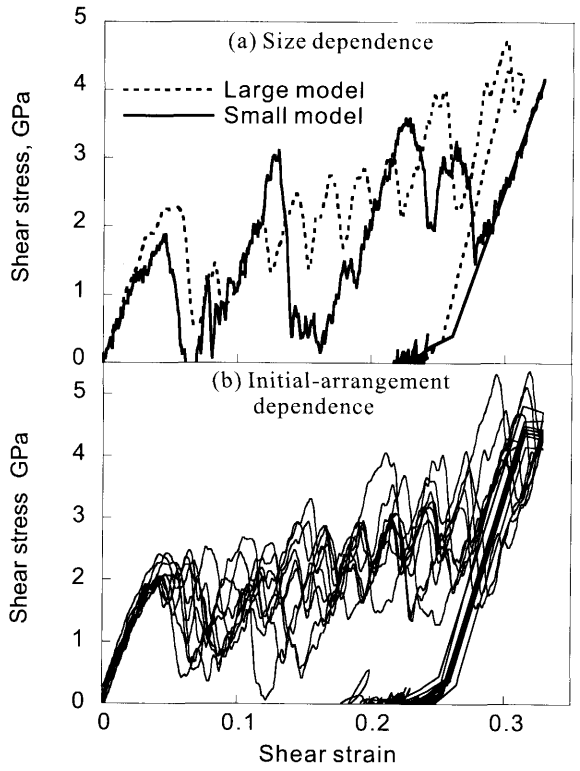


Fig. 8 Stress-strain curves for different-size models (a) and different initial arrangements (b)

Since the random selection of Al atoms is introduced to achieve the 68% Ni composition, the arrangement of the Ni and Al atoms differs in each trial. Figure 8 (b) represents the dependence on the initial arrangement. The peaks and intervals in the loading curve differ for each trial, while the initial gradients of the curves coincide completely. By taking the average of the trials, however, the S-S curve is considered to approach the continuous curve obtained experimentally.

### 4.4 Deformation in variant layer

In the previous model and the L-model in this study,

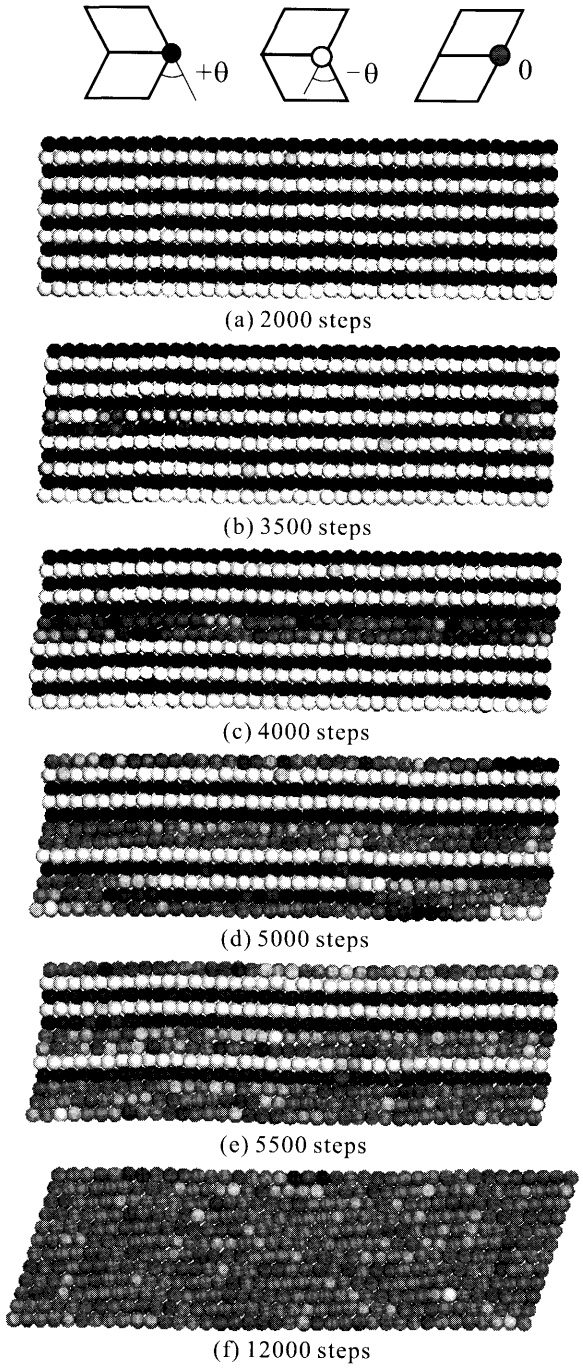


Fig. 9 Progress of deformation in each variant layer



NII-Electronic Library Service

The Japan Society of Mechanical Engineers



the width, or the length of the edge along the variant layer direction, is small, and the deformation in one layer occurs instantaneously. On a large scale, however, simultaneous deformation is energetically difficult. Therefore, a simulation with a three-times wider model (W model in Fig. 5) is carried out, and the result for the loading process is illustrated in Fig. 9. The atoms are shaded corresponding to the angle of the layer. When the layer above and below an atom is in opposite directions, the atom is black or white, and when the layers are in the same directions, the atom is gray. Since the initial martensite layers tilt to the right and left in turn, black and white layers are alternately stacked, as shown in Fig. 9 (a). During elastic deformation, nothing happens. At the 35 000th step, the deformation is initiated at a part in the middle layer, which is shown in Fig. 9 (b) by the color of the left half of the layer becoming gray while the color of the right half remains black or white. This deformed region propagates, and finally, the deformation in the layer completes by the 40 000th step. Similar initiation and propagation occur repeatedly until all layers in the model takes the same direction.

## 5. Concluding Remarks

Molecular dynamics simulations of the shape memory effect were carried out. Overall, a good agreement with a given mechanism was demonstrated, while atomistically, the following results were obtained in this study: Deformation was revealed to occur based on the change in the orientation of variant layers in the martensite phase, and to proceed layer by layer. The stress-strain curve then showed a zigzag shape with oscillation, and the interval of the peaks in the zigzag curve became smaller as model size increased. This kind of oscillation was also observed experimentally[15], although it was much smaller. This difference between MD and macroscopic experiments is, however, expected to be reduced by using a larger model, as inferred from Fig. 8 (a). The in-layer deformation of the martensite phase was also discussed, and the deformation was revealed to be partially initiated and to propagate in the layer in a short time.

Finally, we summarize the points to be improved in future work. The martensite structure is not completely identical to the real structure in Ni-Al alloys. Comparison with the experimental data of the structure, as well as quantitative evaluation of thermophysical properties, such as transformation stress and temperature, should be carried out to discuss more precise behavior. The application of the herein presented method to other shape-memory alloys such as Ni-Ti is also expected[16]. As mentioned in section 4, the model-size dependence is obvious, and the model in this paper is still too small. In a real martensite phase, grains and variants are randomly distributed, and complicated behavior at the grain boundary and variant interface must be considered. Nevertheless, the atomistic behavior obtained in this study is worthwhile in understanding of mechanism and applicable to design of nanodevices using shape memory alloys.

## Acknowledgements

The authors acknowledge Professor Tatsuo Inoue, Fukuyama University, for helpful discussion on the phase transformation mechanism and computational modeling.

## References

(1) Tanaka, K. and Nagaki, S., A Thermomechanical Description of Materials with Internal Variables in the Process of Phase Transformation, Ingenieur-Archiv, Vol.51 (1982), pp.287–299.

(2) Foiles, S.M. and Daw, M.S., Application of the Embedded Atom Method of $Ni_3Al$, J. Mater. Res., Vol.2 (1987), pp.5–15.

(3) Chen, S.P., Srolovitz, D.J. and Voter, A.F., Computer Simulation on Surfaces and [001] Symmetric Tilt Grain Boundaries in Ni, Al, and $Ni_3Al$, J. Mater. Res., Vol.4 (1989), pp.62–77.

(4) Daw, M.S. and Baskes, M.I., Embedded-Atom Method: Derivation and Application to Impurities, Surfaces, and other Defects in Metals, Phys. Rev. B, Vol.29 (1984), pp.6443–6463.

(5) Foiles, S.M., Baskes, M.I. and Daw, M.S., Embedded-Atom-Method Functions for the fcc Metals Cu, Ag, Au, Ni, Pd, Pt, and Their Alloys, Phys. Rev. B, Vol.33 (1986), pp.7983–7991.

(6) Rubini, S. and Ballone, P., Quasiharmonic and Molecular-Dynamics Study of the Martensitic Transformation in Ni-Al Alloys, Phys. Rev. B, Vol.48 (1993), pp.99–111.

(7) Farkas, D., Mutasa, B., Vailhe, C. and Ternes, K., Interatomic Potentials for B2 NiAl and Martensitic Phases, Modelling Simul. Mater. Sci. Eng., Vol.3 (1995), pp.201–214.

(8) Uehara, T. and Tamai, T., Molecular Dynamics Simulations on Shape Memory Effect in Ni-Al Alloy, Proc. 6th World Cong. Comp. Mech., CD-ROM, (2004).

(9) Uehara, T. and Tamai, T., Molecular Dynamics Simulation on Shape-Memory Effect in Ni-Al Alloy by Using EAM Potential, Trans. Jpn. Soc. Mech. Eng., (in Japanese), Vol.71, No.705, A (2005), pp.717–723.

(10) Uehara, T. and Tamai, T., An Atomistic Study on Shape-Memory Effect by Shear Deformation and Phase Transformation, Mechanics of Advanced Materials and Structures, Vol.13 (2006), pp.197–204.

(11) Clementi, E. and Roetti, C., Roothaan-Hartree-Fock Atomic Wavefunctions, Atomic Data and Nuclear Data Tables, Vol.14 (1974), pp.177–478.

(12) Rose, J.H., Smith, J.R., Huina, J. and Ferrante, J., Universal Features of the Equation of State of Metals, Phys. Rev. B, Vol.29 (1984), pp.2963–2969.

(13) Parrinello, M. and Rahman, A., Crystal Structure and Pair Potentials: A Molecular-Dynamics Study, Phys. Rev. Lett., Vol.45 (1980), pp.1196–1199.

(14) Parrinello, M. and Rahman, A., Polymorphic Transitions in Single Crystals: A New Molecular Dynamics Method, J. Appl. Phys., Vol.52 (1981), pp.7182–7190.



NII-Electronic Library Service

The Japan Society of Mechanical Engineers



(15) Leo, P.H., Shield, T.W. and Bruno, O.P., Transient Heat Transfer Effects on the Pseudoelastic Behavior of Shape-Memory Wires, Acta Metall. Mater., Vol.41 (1993), pp.2477–2485.

(16) Sato, T., Saito, K., Uehara, T. and Shinke, N., Molecular Dynamics Study on Nano Structure and Shape-Memory Property of Ni-Ti Alloy, Trans. Mat. Res. Soc. Japan, Vol.29 (2004), pp.3615–3618.



NII-Electronic Library Service